# Chapter 26
# A Benchmark Structure for Validation of Experimental Substructuring, Transfer Path Analysis and Source Characterisation Techniques

**M.V. van der Seijs, E.A. Pasma, D.D. van den Bosch, and M.W.F. Wernsen**

**Abstract** This paper presents a practical study on popular Experimental Dynamic Substructuring topics. A series of substructures is designed of such complexity to fit in right between "real life" structures as often found in industrial applications and "academic" structures which are typically the simplest models to identify a particular phenomenon. The designed benchmark structure comprises an active side with a vibration source, a passive side and a test rig for source characterisation. The connectivity is scalable in complexity, meaning that a single-point, two-point and continuous interface can be established. Substructuring-compatible component models are obtained from impact measurements using the Virtual Point Transformation. The vibration source on the active structure is characterised on the test rig using the in-situ TPA concept. Hereafter the component TPA method is applied to simulate the response on the passive side of the coupled structure, in turn obtained using dynamic substructuring.

**Keywords** Dynamic substructuring • Virtual point transformation • Transfer path analysis • Blocked force • In-situ

## 26.1 Introduction

Dynamic Substructuring (DS), Transfer Path Analysis (TPA) and Source Characterisation (SC) are three research fields that have received tremendous attention from both science and industry. All three aim to provide practical solutions for engineering of structural vibrations and sound, with applications stretching from the automotive and aerospace industry to high-tech precision machinery and sustainable energy solutions. However, it is fair to say that the similarities between the three fields have not always been well understood [1]. This is perhaps motivated by their different origins, for instance: substructuring finds its oldest roots in numerical modelling and reduction of aerospace structures [2–5], transfer path analysis evolved hand-in-hand with automotive NVH engineering [6–10] and source characterisation emerged from fields such as vibration isolation and structure-borne sound engineering [11–15]. Only in recent years, some studies [9, 16–18] have appeared that incorporate various aspects of the three fields, while [19, 20] extend to yet other fields such as feedback control theory.

At the same time, many methods within DS, TPA and SC prove to be rather challenging to validate in the context of an industrial application. This is often due to a myriad of experimental uncertainties (signal-to-noise problems, incomparable operational/boundary conditions, presence of secondary excitation sources, etcetera) on top of the applications' inherent complexities. To avoid such uncertainties and reduce the overall complexity of a problem, studies on "academic" structures are often conducted first, such that the method's key properties present themselves as clearly identifiable and unambiguous properties. And although such studies provide an excellent basis for theory development, it remains difficult to transpose a proof of a theoretical concept to application on an industrial problem.

M.V. van der Seijs (✉) • E.A. Pasma • D.D. van den Bosch
VIBES.technology, Molengraaffsingel 14, 2629, Delft, The Netherlands
e-mail: maarten@vibestechnology.com

M.W.F. Wernsen
VIBES.technology, Molengraaffsingel 14, 2629, Delft, The Netherlands

Department of Precision and Microsystems Engineering, Delft University of Technology, Mekelweg 2, 2628CD, Delft, The Netherlands



M.S. Allen et al. (eds.), *Dynamics of Coupled Structures, Volume 4*, Conference Proceedings of the Society for Experimental Mechanics Series, DOI 10.1007/978-3-319-54930-9_26

### 26.1.1 Paper Goal and Outline

The goal of this paper is twofold. First, a benchmark structure is proposed of such complexity, that it fits in right between the "real-life" industrial structures on the one hand, and the limited-DoF academic examples on the other hand. Section 26.2 introduces the three benchmark substructures: an active, passive and test rig substructure. The benchmark substructures have been designed to allow for three different coupling configurations with increasing interface complexity.

The second goal of this paper is to apply concepts of DS, TPA and SC using measurements on the constructed benchmark structures. Section 26.3 presents a high-level overview of a selection of possible applications, including a virtual point transformation, coupling of substructures A and B, source characterisation of A in test assembly AR and transfer path analysis for prediction of vibrations in assembly AB.

## 26.2 Benchmark Design

The benchmark construction has been motivated by the desire to validate methods within the fields of experimental DS and TPA. More specifically, the aim was to experiment with methods as covered in the general framework articles on the two topics, respectively [5] and [1]. In the latter one, three types of substructures are used for theory development: an active source structure, a passive receiving structure and a test rig for source characterisation. These three substructures have formed the basis for the benchmark. Also, as the interest is in validating methods in a frequency range of 0–5000 Hz, the benchmark substructures are supposed to display sufficient dynamics (i.e. vibration modes) in this range.

### 26.2.1 Substructure Design

Figure 26.1 shows the three substructures. Let us introduce them one by one and briefly touch upon some design considerations:

- Substructure A is welded together from three pieces of solid aluminium (30×30 mm). It forms an evenly sided triangle and loosely resembles the character 'A', but was made asymmetric to avoid double resonance modes. It comprises a number of 10 mm diameter holes, at the corner points and along the length of the members, evenly spaced at distances of 75 mm. It hosts a vibration source (further discussed below) and can therefore represent the active source system in a TPA or SC problem. The combined weight is circa 2.5 kg.
- Substructure B is constructed from two plates of stainless steel with a solid piece of steel welded in between. The plates are produced using precise laser-cutting. Five holes are placed spanning a total distance of 300 mm, again with 75 mm spacing in between. A honeycomb-like pattern of cuts was introduced to reduce weight, as well as to provide a pattern to align sensors for an observability investigation.[1] As such, substructure B represents a receiving side into which the source vibrations of substructure A may propagate. The total weight is circa 10 kg.
- Substructure R is a collection of small identical support structures, together forming a test rig for testing of substructure A. The supports are machined from solid aluminium blocks and can be mounted on a wooden base plate. An opening in the centre was made to reduce the stiffness of the top with respect to the fixed base. The test rig R can be used to characterise the source vibrations of substructure A, for prediction of vibrations in an assembly with substructure B. The weight of each support is 670 gramme.

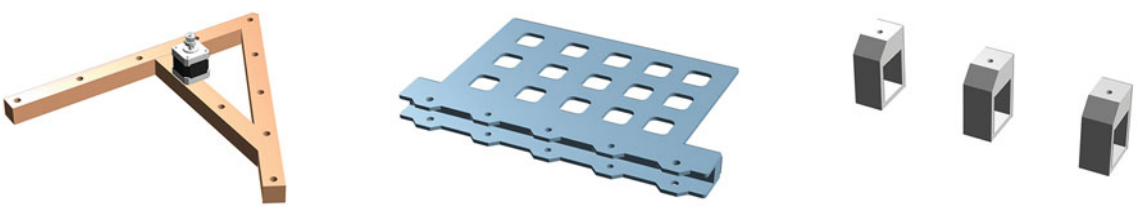

**Fig. 26.1** The three benchmark substructures: active source A (*left*), passive receiver B (*centre*) and test rig parts R (*right*)

[1] See the paper in the proceedings of SEM IMAC 2017: *M. Wernsen et al. An indicator sensor criterion for in-situ characterisation of source vibrations*.

### 26.2.2 Vibration Source

For application of SC and TPA, substructure A needs to have an active vibration source. Many applied studies in this field report on difficulties with maintaining identical operational conditions throughout the various testing environments [9, 21–23]. In the definition of the benchmark, it has therefore been a key requirement to have a source that generates perfectly reproducible vibrations. Other requirements were to have a source with distinct orders, i.e. a very constant speed with a stationary excitation profile, and an excitation spectrum that renders sufficient signal-to-noise in the frequency range of interest.

The chosen vibration source is a NEMA 17 stepper motor: a typical electric motor used in 3D printing hardware. The stepper is controlled using an Arduino DUE with a Pololu A4988 stepper motor driver. It uses a PWM protocol for speed control, which can be programmed to run through various speeds. In contrast to e.g. an AC electric motor, a stepper motor has a rather 'rippled' rotational speed profile, generating a lot of motor orders, i.e. harmonics proportional to the fundamental frequency. If desired, an unbalance mass can be connected to the shaft of the motor to further amplify the vibration amplitude. The PWM signal can be connected to a tacho-pulse channel of a DAQ system, allowing for accurate speed monitoring during operational measurement.

### 26.2.3 Assembly Variants

The individual substructures have been designed to allow for multiple assembly configurations. Figure 26.2 shows these assemblies for AB (top) and AR (bottom). The configurations respectively represent a single coupling point, two coupling points and five coupling points, the latter resembling a continuous interface. In all cases, standard M10 bolts and nuts can be inserted to fasten the structures.

- The single-point configuration is meant to be the simplest assembly to comprehend from a structural-dynamic point of view. Although both structures comprise dozens of modes in a bandwidth of 5 kHz, one might reason that only six vibration modes can be transferred over the interface. Substructure coupling of A and B would thus imply writing an interface condition for the three translational and three rotational DoFs. The single-point configuration is well suited to investigate e.g. experimental substructure coupling and decoupling [24, 25].
- The two-point configuration roughly doubles the complexity of the assembly. Following the same reasoning, a maximum of 12 vibration modes would now be present in the vibration transfer between A and B. However, it is evident that there is interplay between the two coupling points, which deserves special attention in any application of substructuring or force identification. Indeed, the two-point coupling configuration forms a perfect basis to study phenomena related to interface conditioning, such as matrix regularisation and observability of the interface vibrations.

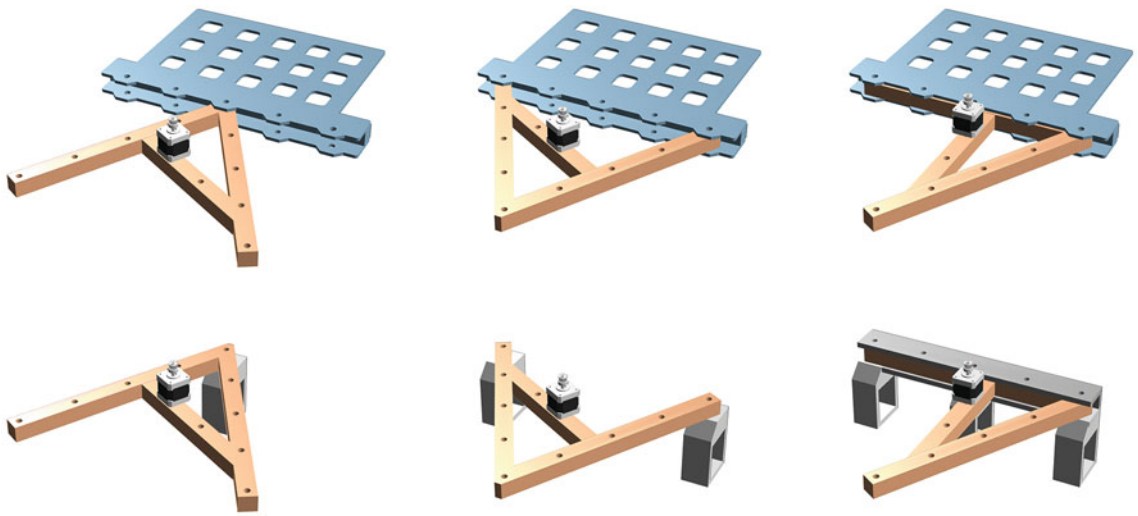

**Fig. 26.2** Various configurations of the benchmark structures. *Upper row*: assemblies of A and B in 1/2/5-point configuration. *Lower row*: assemblies of A and R in 1/2-point configuration

– The five-point configuration resembles a continuous interface. In this case, it is likely that the effect of each coupling point can no longer be distinguished. Instead, the combined interface effect would probably be best considered in terms of modes. Modal substructuring techniques such as [26] can be tested on this assembly, as well the transmission simulator method [27].

The entire benchmark collection provides an abundance of data for investigation of many DS, SC and TPA topics, which shall be the topic of the next section.

## 26.3 Applications

The coming sections provide a high-level overview of some experimental applications. Examples are shown of experimental modelling using virtual point transformation, dynamic substructuring, source characterisation and transfer path analysis. In order not to dwell in theory, the derivations and equations have been kept to a minimum. Reference is made to original literature for the interested reader.

For the purpose of this study, an extended range of assemblies has been subjected to impact hammer and operational measurements. Figure 26.3 shows two of those assemblies: AB in single-point and AR in two-point coupling configuration. All separate substructures and the assemblies AB have been measured in free-floating conditions, i.e. suspended by soft springs. The assemblies AR have been mounted onto a wooden base plate, in turn resting on a test table on air springs.

### *26.3.1 Experimental Modelling*

Experimental modelling can be understood as the art of obtaining a structural-dynamic model (such as FRFs) from measurements [18, 28, 29]. It constitutes a fundamental step in experimental substructuring, but also finds application in component transfer path analysis. This section briefly discusses how a nodal FRF model can be obtained from impact hammer measurements, demonstrated for experimental modelling of substructures A and B.

#### 26.3.1.1 Short Theory of the Virtual Point Transformation

Typically, experimentally obtained models lack a common interface which allows for substructure coupling. In the numerical domain, nodes provide this common interface, as a direct result of FE modelling (sometimes after remeshing or a node collocation technique [30]). The Virtual Point Transformation [29] introduces such nodes in experimentally obtained models.

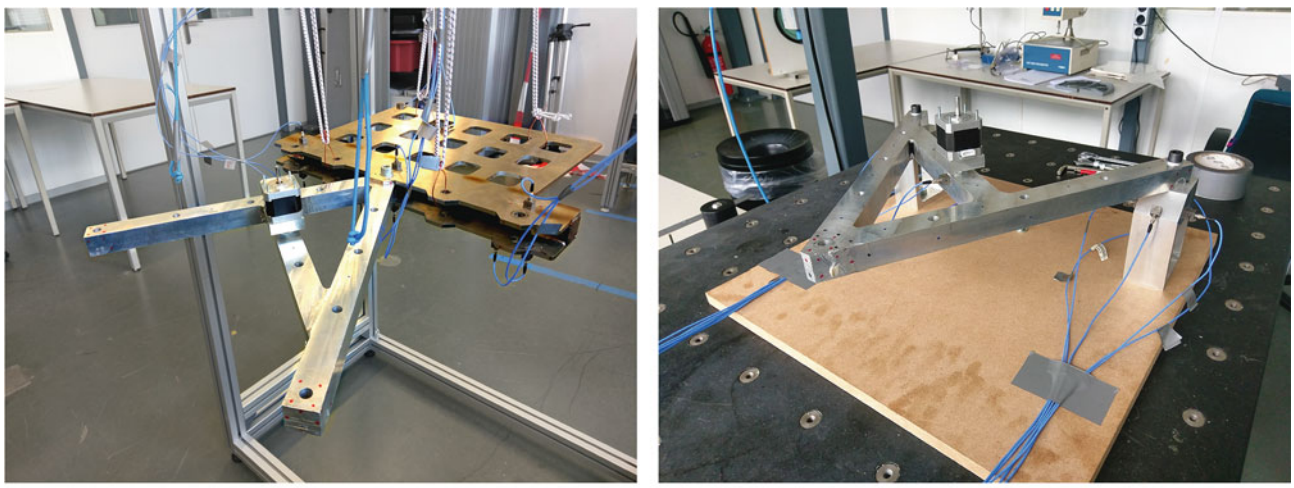


**Fig. 26.3** Two test configurations. (**a**) Assembly AB in the single-point coupling configuration, free-floating suspended by soft springs. (**b**) Assembly AR in the two-point coupling configuration, mounted to a wooden base plate resting on a test table

The main idea is to choose a point on or near a physical interface of a substructure that can be made compatible with the other (experimental or numerical) substructure to couple. All measured displacements $\mathbf{u}$ and forces $\mathbf{f}$ around the interface can be transformed to this virtual point, resulting in a 6-DoF 'nodal' description consisting of virtual translations/rotations $\mathbf{q}$ and forces/moments $\mathbf{m}$:

$$\text{Displacements}: \quad \mathbf{u} = \mathbf{R_u q} \quad \Longrightarrow \quad \mathbf{q} = (\mathbf{R_u})^+ \mathbf{u} \qquad \mathbf{R_u} \in \mathbb{R}^{n\times 6} \tag{26.1a}$$

$$\text{Forces}: \quad \mathbf{m} = \mathbf{R_f^T f} \quad \Longrightarrow \quad \mathbf{f} = \left(\mathbf{R_f^T}\right)^+ \mathbf{m} \qquad \mathbf{R_f} \in \mathbb{R}^{m\times 6} \tag{26.1b}$$

The two transformations allow to compute a $6\times 6$ virtual point FRF matrix $\mathbf{Y_{qm}}(\omega)$ from a measured $n\times m$ matrix $\mathbf{Y}(\omega)$. This can easily be set up for each coupling point, building a experimental 'super-element' that is compatible for substructuring with other models:

$$\text{Measured FRFs}: \quad \mathbf{u} = \mathbf{Y f} \tag{26.2a}$$

$$\text{Virtual point FRFs}: \quad \mathbf{q} = (\mathbf{R_u})^+ \mathbf{Y} \left(\mathbf{R_f^T}\right)^+ \mathbf{m} \quad \Longrightarrow \quad \mathbf{q} = \mathbf{Y_{qm} m} \tag{26.2b}$$

One underlying assumption of this transformation is that the measured substructures behave rigidly in the vicinity of this interface in the frequency range of interest [29]. This assumption and other criteria will be discussed next.

#### 26.3.1.2 FRF Measurement

All substructure FRFs have been obtained by impact hammer testing. Figure 26.4 depicts how hammer impact points (red arrows) and tri-axial accelerometers (grey cubes) have been positioned and oriented on substructures A and B. Besides some internal points, the main interest for both substructures are the three coupling points. Each coupling point has been instrumented by 3 tri-axial accelerometers of type PCB 356B21. To determine forces and moments, 16 impact hammer positions are chosen per coupling point. Altogether, this results in sufficient overdetermination of the virtual point transformations.

#### 26.3.1.3 FRF Consistency

In order to evaluate the above assumption on rigidity and obtain insight in the contribution of single force impacts or displacements to the VP dynamics, several consistency checks can be done. With a consistency check, the experimentally obtained results are first transformed to the virtual point and then expanded (or projected) back on the original measured DoFs [18, 29]. The difference in the original response and the projected response provides inside on how much residual

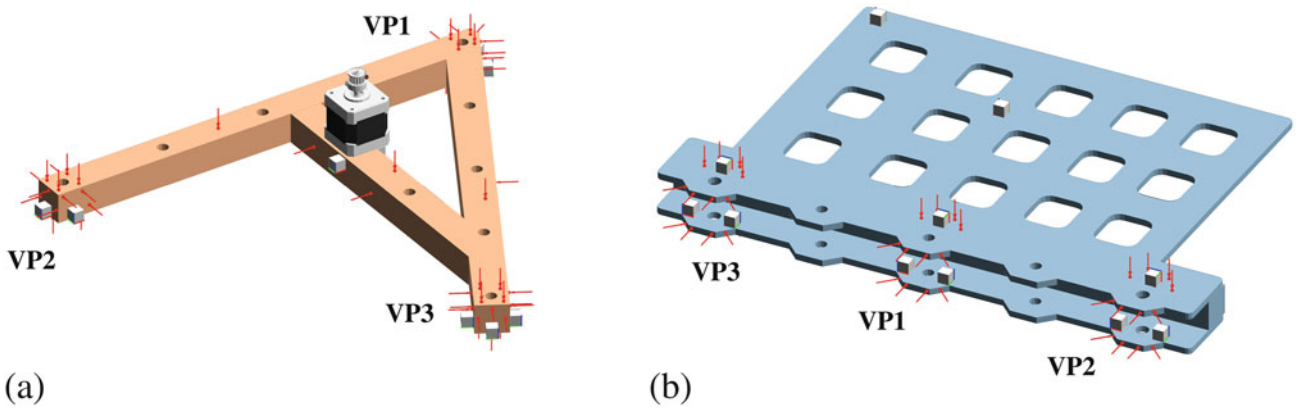


**Fig. 26.4** Acceleration sensors (indicated by *grey cubes*) and impact locations (*red arrows*) visualised on the substructures. (**a**) Substructure A. The three coupling points are each instrumented by 3 tri-axial accelerometers and 16 impact points. (**b**) Substructure B. The three coupling points are each instrumented by 3 tri-axial accelerometers and 16 impact points; 2 additional sensors register target responses in the structure

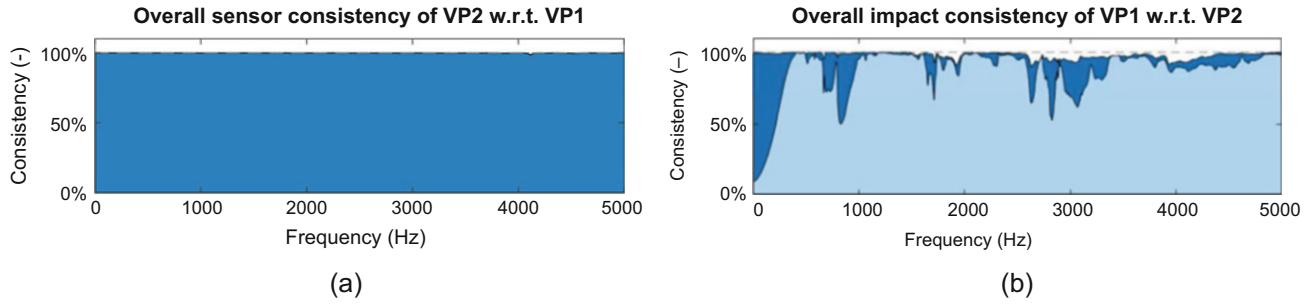


**Fig. 26.5** Sensor and impact consistency checks for substructure A. (**a**) Overall sensor consistency of 9 sensor channels around VP2 with respect to excitations around VP1. (**b**) Overall impact consistency of 16 (*light blue*) and 13 (*blue*) impacts out of 16 around VP1 with respect to responses around VP2

dynamics (interface flexibility) has been neglected with the virtual point transformation. More practically, this technique is used to evaluate the contribution of single measured DoFs to the transformed VP dynamics. This can be used to find erroneous definitions of sensor and impact positions or directions in the transformation, or discard 'bad impacts'[2] from the transformation.

Let us illustrate the various consistency checks for substructure A. Figure 26.5a shows the overall sensor consistency of VP2 for excitations around VP1. This operation takes the accelerances of all 9 sensors channels (FRF matrix rows) around VP2 ($\mathbf{u}$) for a combination of hammer impacts (FRF matrix columns) around VP1, transforms these to the virtual point $\mathbf{q}$ and expands the accelerances back to their original sensor channels ($\tilde{\mathbf{u}}$). The score of 100% over the full bandwidth of 5000 Hz indicates that all sensor channels are perfectly consistent, i.e. $\tilde{\mathbf{u}} = \mathbf{u}$. This is obvious as the region between the three sensors is very stiff; values below 100% would probably indicate incorrect placement of a sensor.

Figure 26.5b shows the overall impact consistency for VP1 with respect to responses around VP2. The light-blue area was computed for all 16 impact points, which is clearly not optimal. Looking into the specific impact consistency for each 16 impacts, three impacts had significant lower score than average. By discarding these 3 from the set of 16, the full 6-DoF set of virtual point forces/moments can still be determined. The dark-blue area was computed for the optimised set, clearly showing an improved overall impact consistency.

#### 26.3.1.4 FRF Reciprocity

The VP transformation allows to validate reciprocity of the obtained virtual point FRFs, as computed by Eq. (26.2b). Note that this is possible as the VP displacements (i.e. linear and rotational accelerations) are perfectly 'vectorially associated' with the corresponding VP loads (i.e. forces and moments). In other words, the virtual point FRFs behave as if they were computed for nodes of an FE model.

Figure 26.6 shows two typical virtual point FRFs: response VP2Y over force VP3Y of substructure A (left) and response VP2Z over force VP3Z of substructure B (right). The FRFs reciprocal FRFs are displayed in red. It can be observed that reciprocity is indeed satisfied, especially up to 2 kHz.

### *26.3.2 Dynamic Substructuring*

Now that VP transformed FRFs are available for substructure A and B, both structures are coupled using the LM-FBS algorithm [5, 31]. To do so, the substructure FRF matrices of A and B are put in block-diagonal form and an appropriate Boolean matrix $\mathbf{B}$ is written (not discussed here):

$$\tilde{\mathbf{Y}} = \mathbf{Y} - \mathbf{Y}\mathbf{B}^T \left(\mathbf{B}\mathbf{Y}\mathbf{B}^T\right)^{-1} \mathbf{B}\mathbf{Y} \qquad \mathbf{Y} \triangleq \begin{bmatrix} \mathbf{Y}^{\mathrm{A}} & \mathbf{0} \\ \mathbf{0} & \mathbf{Y}^{\mathrm{B}} \end{bmatrix} \tag{26.3}$$

[2] Bad impacts can for instance be caused by a low impact energy in the frequency range of interest, low signal-to noise ratio, poor reachability with an impact hammer due to geometric constraints, double pulses, etcetera.

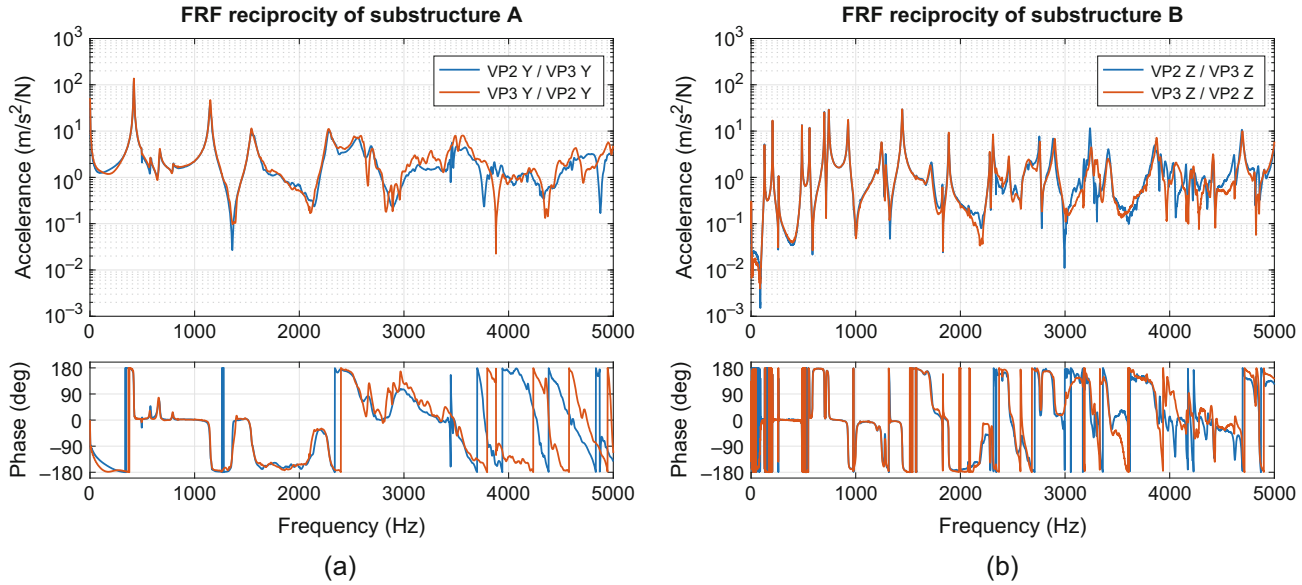


**Fig. 26.6** Reciprocity of the virtual point FRFs of the experimental models of substructure A and B. (**a**) Substructure A: Y-direction of VP2 to VP3 and its reciprocal. (**b**) Substructure B: Z-direction of VP2 to VP3 and its reciprocal

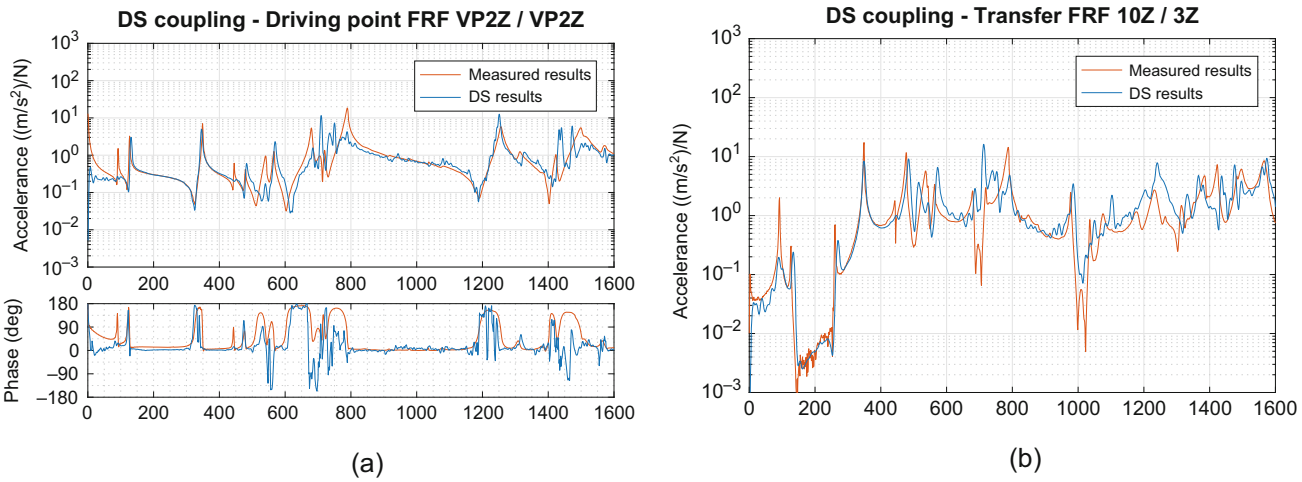


**Fig. 26.7** Application of dynamic substructuring: assembled FRFs of AB (*blue*) in two-point coupling configuration, compared against the validation measurement (*red*). (**a**) Driving-point FRF for VP3 in Z-direction. (**b**) Transfer FRF for an internal impact point on A to an internal acceleration response on B, both in Z-direction

The two-point coupling configuration is considered, which means that coupling is performed by requiring strict coordinate compatibility and force equilibrium for the FRFs of virtual points 2 and 3. We now focus on the frequency range of 0–1600 Hz.

Some results of the substructured FRFs of AB are depicted in Fig. 26.7. First in Fig. 26.7a, a driving point FRF on the coupling interface is shown, namely for VP2 in Z-direction. The phase is shown as well to assess the passivity[3] of the FRF. Figure 26.7b shows a transfer FRF from an internal force impact point on structure A to an acceleration response internally on structure B. Both points are not part of a coupling VP, hence the transfer FRF is realised by coupling over the interface. The substructured FRFs (blue) are compared the measured FRFs of the coupled structure AB.

[3]For an accelerance driving point FRF, the phase should be bounded by 0 and +180°.

The first substructuring results, although not perfect yet, are by all means encouraging. It can be seen how resonance frequencies are created at roughly the right frequencies. The phase around anti-resonances is not fully stable, however the overall amplitude of the FRFs match quite well. Note that no filtering or processing has been applied to the measured FRF data, except for transformation to virtual points.

### 26.3.3 In-Situ Source Characterisation

To characterise the active vibrations of source structure A, the in-situ characterisation method is used [15]. This method describes the source structure using 'blocked forces' on its interfaces (as if the component were connected to a fully rigid boundary) by measuring operational responses on a connected receiver structure. More specifically, this method is able to characterise a source structure in an assembly, with the resulting characterisation being a property of the source structure only rather than being a property of the combined assembly. Because this characterisation is a source-inherent property, the obtained blocked forces are transferable to other receiving structures. Therefore, in theory, the source may be characterised in the original assembly (e.g. AB) or on a test rig with different dynamic properties (e.g. AR). This paper shows examples of both variants.

The in-situ source characterisation method comprises three steps. Here, it is discussed for the test rig variant; for more explanation of the notation and terminology used, see [1].

1. Operational measurement of the source structure A mounted to a test rig R where indicator responses $\mathbf{u}_4$ on test rig R are measured (see the test setup in Fig. 26.3b);
2. FRF measurement of the combined structure AR, more specifically from force inputs at the interface $\mathbf{f}_2$ to the indicator responses on the test rig $\mathbf{u}_4$. Here it is key that the DoFs $\mathbf{u}_4$ are the same set as with the operational measurement;
3. Characterisation of the active source by means of a matrix-inverse operation, resulting in blocked forces for each operational measurement cycle:

$$\mathbf{f}_2^{\mathrm{eq}} = \left(\mathbf{Y}_{42}^{\mathrm{AR}}\right)^{+} \mathbf{u}_4 \tag{26.4}$$

where $\mathbf{f}_2^{\mathrm{eq}}$ denotes the blocked forces representing the source structure, $\mathbf{u}_4$ the measured operational responses of step 1 and $\mathbf{Y}_{42}^{\mathrm{AR}}$ the FRFs of the source on test rig measured in step 2.

Note that if a virtual point transformation to a 6-DoF description is done on the force input side of the FRF matrix (i.e. the columns of $\mathbf{Y}_{42}$ relate to forces and moments in virtual point format), the resulting blocked forces $\mathbf{f}_2^{\mathrm{eq}}$ will also present themselves in this form, making them easily transferable to other structures. In other words, one would obtain a source characterisation comprising three forces and three moments per coupling point, instead of a series of only translational forces.

The source vibrations of the active structure A have been characterised in the original 'target' assembly with passive side B *and* on the test rig structure R. Hence, the two in-situ characterisations yield two sets of 12 blocked forces/moments: 6 for each coupling point. These sets are used for vibration prediction in target assembly AB, which is presented in the next section.

### 26.3.4 Component-Based Transfer Path Analysis

For the purpose of virtual noise and vibration prediction (sometimes called Virtual Acoustic Prototyping, [32]), component Transfer Path Analysis is applied on the benchmark data. The advantage of component TPA is the ability to predict target response levels $\mathbf{u}_3$ in/on a passive structure B using an independent source characterisation (i.e. blocked forces) of a source A.

The governing equation of component TPA is as follows:

$$\mathbf{u}_3 = \mathbf{Y}_{32}^{\mathrm{AB}} \mathbf{f}_2^{\mathrm{eq}} \tag{26.5}$$

where $\mathbf{f}_2^{\mathrm{eq}}$ is a set of equivalent/blocked forces for instance obtained by Eq. (26.4) and $\mathbf{Y}_{32}^{\mathrm{AB}}$ the FRF matrix of assembly AB from the interfaces to the responses of interest $\mathbf{u}_3$ (sometimes called Noise Transfer Functions). Combining this with Dynamic Substructuring, one can predict the vibration levels as described above without ever physically assembling structures A

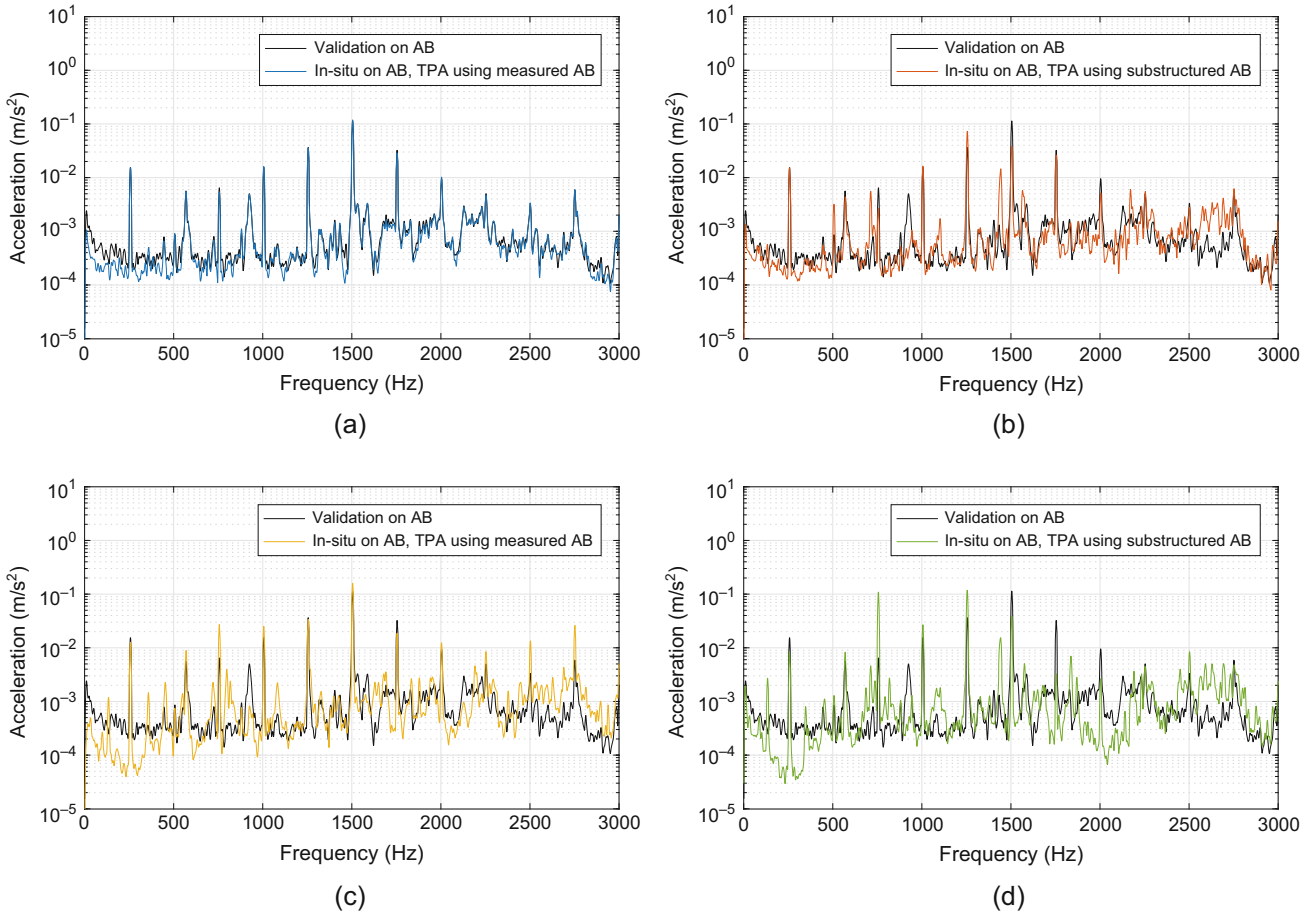


**Fig. 26.8** Four results of in-situ source characterisation and TPA prediction (*blue*/*red*/*yellow*/*green*), all compared to a validation measurement in structure AB (*black*). (**a**) In-situ on AB, TPA prediction using measured FRFs of AB. (**b**) In-situ on AB, TPA prediction using substructured FRFs of AB. (**c**) In-situ on AR, TPA prediction using measured FRFs of AB. (**d**) In-situ on AR, TPA prediction using substructured FRFs of AB

and B [16]. In practice, this allows for a separation in development process, since two parties are able to work on their own structures A and B and an interface is provided in terms of blocked forces, possibly in the format of Virtual Point forces and moments.

Four results of component TPA are shown in Fig. 26.8, namely for source characterisation in AB (top) and AR (bottom) and for component TPA using a measured set of FRFs of AB (left) and substructured FRFs obtained by coupling of A and B (right). A validation response measurement is added for comparison, which is identical for all four plots. Remind that all characterisations are expressed in virtual point blocked forces and moments, i.e. 12 DoFs in total.

The first result in Fig. 26.8a constitutes the most literal application of in-situ TPA: the source is characterised in the original assembly AB, after which the virtual point blocked forces and moments are applied to the same assembly. Near identical results are obtained, especially at the peaks corresponding to the actual signal (source vibration orders) of the stepper motor. Figure 26.8b shows an application of the same blocked forces to the substructured FRFs of assembly AB. Most peaks are well approximated, which may be considered a very good result considering the various substructure FRF measurements involved (A, B and AB). Note that this approach goes into the direction of virtual vibration prototyping, which heavily relies on the virtual point transformation to provide common interfaces between the various measurements.

The results of Fig. 26.8c, d present similar results as above, yet for source characterisations calculated from operational measurements on the test rig. The imposed challenge here is that the test rig structure R possesses very different dynamic properties than B, resulting in totally different operational indicator responses ($\mathbf{u}_4^{\mathrm{AR}}$) than in the original assembly ($\mathbf{u}_4^{\mathrm{AB}}$). It is thus interesting to investigate if a source characterisation can be determined that renders similar responses on another passive side, i.e. is *transferable* to arbitrary assemblies.

Figure 26.8c on the left depicts the test rig characterisation applied to the measured FRF of AB. The results are encouraging, as many peaks that exceed the signal noise floor find roughly the right order of magnitude. The noise floor,

indeed, has been a limiting factor in this measurement, as the signal on the test rig sensors hardly exceeded the noise level. Finally, Fig. 26.8d shows what might be considered the holy grail of component TPA: a characterisation of source vibrations on a test rig, applied to an experimental model of the target assembly obtained using dynamic substructuring. This indeed constitutes a novelty in experimental DS and TPA, and shall be a direction for further investigation.

## 26.4 Conclusions and Outlook

In this paper, a series of benchmark substructures has been presented for method development and validation in the field of DS, TPA and SC. The three benchmark substructures can be connected in several ways, which makes the complexity of the interface problem adjustable to a one-point, two-point or continuous connection. Several applications have been shown to validate methods of experimental modelling, virtual point transformation, dynamic substructuring and source characterisation. Many more validations can be done, which is topic of further research at VIBES.technology.

## References

1. van der Seijs, M.V., de Klerk, D., Rixen, D.J.: General framework for transfer path analysis: history, theory and classification of techniques. Mech. Syst. Signal Process. **68–69**, 217–244 (2016). doi:10.1016/j.ymssp.2015.08.004
2. Hurty, W.C.: Vibrations of structural systems by component mode synthesis. J .Eng. Mech. Div. **86**(4), 51–70 (1960)
3. Craig, R.R.J., Bampton, M.C.C.: Coupling of substructures using component mode synthesis. AIAA J. **6**(7), 1313–1319 (1968). doi:10.2514/3.2947
4. Rubin, S.: Improved component-mode representation for structural dynamic analysis. AIAA J. **13**(8), 995–1006 (1975). doi:10.2514/3.60497
5. de Klerk, D., Rixen, D.J., Voormeeren, S.N.: General framework for dynamic substructuring: history, review and classifcation of techniques. AIAA J. **46**(8), 1169–1181 (2008). doi:10.2514/1.33274
6. Plunt, J.: Finding and fixing vehicle NVH problems with transfer path analysis. Sound Vib. **39**(11), 12–16 (2005)
7. van der Auweraer, H., Mas, P., Dom, S., Vecchio, A., Janssens, K., van de Ponseele, P.: Transfer path analysis in the critical path of vehicle refinement: the role of fast, hybrid and operational path analysis. Technical report 2007-01-2352, SAE technical paper (2007). doi:10.4271/2007-01-2352
8. Sjövall, P.: Identification and Synthesis of Components for Vibration Transfer Path Analysis. Chalmers University of Technology, Gothenburg (2007)
9. de Klerk, D.: Dynamic response characterization of complex systems through operational identification and dynamic substructuring. Ph.D. thesis, Delft University of Technology (2009)
10. Scheuren, J., Lohrmann, M.: Transfer path analysis – experiences, expectations and perspectives. In: International Noise and Vibration Colloquium. SAE Brazil, Sao Paulo (2014)
11. Mondot, J.M., Petersson, B.A.T.: Characterization of structure-borne sound sources: the source descriptor and the coupling function. J. Sound Vib. **114**(3), 507–518 (1987). doi:10.1016/S0022-460X(87)80020-2
12. Petersson, B.A.T., Gibbs, B.M.: Use of the source descriptor concept in studies of multi-point and multi-directional vibrational sources. J. Sound Vib. **168**(1), 157–176 (1993). doi:10.1006/jsvi.1993.1367
13. ISO Technical Committee 43/Subcommittee 1/Workgroup 22 (ISO/TC43/SC1/WG22): Acoustics – characterization of sources of structure-borne sound with respect to sound radiation from connected structures – measurement of velocity at the contact points of machinery when resiliently mounted, ISO 9611, International Standards Organisation (1996)
14. Moorhouse, A.T.: On the characteristic power of structure-borne sound sources. J. Sound Vib. **248**(3), 441–459 (2001). doi:10.1006/jsvi.2001.3797
15. Moorhouse, A.T., Elliott, A.S., Evans, T.A.: In situ measurement of the blocked force of structure-borne sound sources. J. Sound Vib. **325**(4–5), 679–685 (2009). doi:10.1016/j.jsv.2009.04.035
16. Rixen, D.J., Boogaard, A., van der Seijs, M.V., van Schothorst, G., van der Poel, T.: Vibration source description in substructuring: a theoretical depiction. Mech. Syst. Signal Process. **60–61**, 498–511 (2015). doi:10.1016/j.ymssp.2015.01.024
17. Madsen, M.B.: Electrical power assisted steering – dynamic source strength characteristic and vehicle NVH prediction. Master's thesis, University of Southern Denmark (2014)
18. van der Seijs, M.V.: Experimental dynamic substructuring: analysis and design strategies for vehicle development. Ph.D. thesis, Delft University of Technology (2016). doi:10.4233/uuid:28b31294-8d53-49eb-b108-284b63edf670
19. Botelho, R.M., Christenson, R.E.: Mathematical equivalence between dynamic substructuring and feedback control theory. In: Dynamics of Coupled Structures. Proceedings of the 33rd IMAC, A Conference and Exposition on Structural Dynamics, vol. 4, chapter 3, pp. 31–40. Springer, New York (2015). doi:10.1007/978-3-319-15209-7_4
20. Franco, J.A., Botelho, R.M., Christenson, R.E.: Controls based hybrid sub-structuring approach to transfer path analysis. In: Dynamics of Coupled Structures. Proceedings of the 34rd IMAC, A Conference and Exposition on Structural Dynamics, vol. 4, chapter 3, pp. 15–24. Springer, New York (2016). doi:10.1007/978-3-319-29763-7_3
21. Elliott, A.S., Moorhouse, A.T., Huntley, T., Tate, S.: In-situ source path contribution analysis of structure borne road noise. J. Sound Vib. **332**(24), 6276–6295 (2013). doi:10.1016/j.jsv.2013.05.031

22. van der Seijs, M.V., Pasma, E.A., de Klerk, D., Rixen, D.J.: A comparison of two component TPA approaches for steering gear noise prediction. In: Dynamics of Coupled Structures. Proceedings of the 33rd IMAC, A Conference and Exposition on Structural Dynamics, vol. 4, chapter 7, pp. 71–79. Springer, New York (2015). doi:10.1007/978-3-319-15209-7_7
23. Lennström, D., Olsson, M., Wullens, F., Nykänen, A.: Validation of the blocked force method for various boundary conditions for automotive source characterization. Appl. Acoust. **102**, 108–119 (2016). doi:10.1016/j.apacoust.2015.08.019
24. D'Ambrogio, W., Fregolent, A.: Decoupling procedures in the general framework of frequency based substructuring. In: Proceedings of the XXVII International Modal Analysis Conference (IMAC), Orlando. Society for Experimental Mechanics, Bethel (2009)
25. Voormeeren, S., Rixen, D.: A family of substructure decoupling techniques based on a dual assembly approach. Mech. Syst. Signal Process. **27**(18), 379 (2012). doi:10.1016/j.ymssp.2011.07.028
26. Allen, M., Mayes, R., Bergman, E.: Experimental modal substructuring to couple and uncouple substructures with flexible fixtures and multi-point connections. J. Sound Vib. **329**(23), 4891–4906 (2010). doi:10.1016/j.jsv.2010.06.007
27. Mayes, R.L., Rohe, D.P.: Coupling experimental and analytical substructures with a continuous connection using the transmission simulator method. In: Topics in Experimental Dynamic Substructuring. Proceedings of the 31st IMAC, A Conference on Structural Dynamics, vol. 2, chapter 10, pp. 123–135. Springer, New York (2013). doi:10.1007/978-1-4614-6540-9_10
28. Wikipedia, Dynamic substructuring – Wikipedia, the free encyclopedia (2016). Accessed July 2016
29. van der Seijs, M.V., van den Bosch, D.D., Rixen, D.J., de Klerk, D.: An improved methodology for the virtual point transformation of measured frequency response functions in dynamic substructuring. In: Papadrakakis, M., Papadopoulos, V., Plevris, V. (eds.) 4th ECCOMAS Thematic Conference on Computational Methods in Structural Dynamics and Earthquake Engineering (COMPDYN), Kos Island, pp. 4334–4347 (2013). doi:10.13140/RG.2.1.2715.3126
30. Voormeeren, S.N.: Dynamic substructuring methodologies for integrated dynamic analysis of wind turbines. Ph.D. thesis, Delft University of Technology (2012). doi:10.4233/uuid:f45f0548-d5ec-46aa-be7e-7f1c2b57590d
31. de Klerk, D., Rixen, D., de Jong, J.: The frequency based substructuring method reformulated according to the dual domain decomposition method. In: Proceedings of the XXIV International Modal Analysis Conference (IMAC), St. Louis. Society for Experimental Mechanics, Bethel (2006)
32. Moorhouse, A.T., Seiffert, G.: Characterisation of an airborne sound source for use in a virtual acoustic prototype. J. Sound Vib. **296**(1–2), 334–352 (2006). doi:10.1016/j.jsv.2006.03.017